



International Journal of Mining, Reclamation and Environment

ISSN: (Print) (Online) Journal homepage: <https://www.tandfonline.com/loi/nsme20>

Intelligent driving system at opencast mines during foggy weather

Sushma Kumari, Monika Choudhary, Khushboo Kumari, Virendra Kumar, Abhishek Chowdhury, Swades Kumar Chaulya, Girendra Mohan Prasad & Sujit Kumar Mandal

To cite this article: Sushma Kumari, Monika Choudhary, Khushboo Kumari, Virendra Kumar, Abhishek Chowdhury, Swades Kumar Chaulya, Girendra Mohan Prasad & Sujit Kumar Mandal (2021): Intelligent driving system at opencast mines during foggy weather, International Journal of Mining, Reclamation and Environment, DOI: [10.1080/17480930.2021.2009724](https://doi.org/10.1080/17480930.2021.2009724)

To link to this article: <https://doi.org/10.1080/17480930.2021.2009724>



Published online: 05 Dec 2021.



Submit your article to this journal 



View related articles 



View Crossmark data 



Intelligent driving system at opencast mines during foggy weather

Sushma Kumari, Monika Choudhary, Khushboo Kumari, Virendra Kumar, Abhishek Chowdhury, Swades Kumar Chaulya, Girendra Mohan Prasad and Sujit Kumar Mandal

Mine Mechanization, Automation, and Technology Development Group, CSIR-Central Institute of Mining and Fuel Research, Dhanbad, India

ABSTRACT

The fog in mining operations minimises the visibility, preventing drivers from a clear view, causing accidents and vehicle collisions. This paper provides an intelligent driving system for heavy earthmoving machinery operators in opencast mines, including hardware and software. Hardware contains high definition and thermal cameras, a global navigation satellite system (GNSS), radar, laser light, wireless devices, graphical processing unit, touch screen, etc. The software covers image stitching, image enhancement, and convolution neural network-based object detection. The display dashboard is divided into four windows. Each window represents a different view, i.e. 180° panorama view of the driving lane, GNSS tracking map, proximity radar detection view, and rear thermal camera view. An additional colour transfer method has been used in the existing image stitching method to reduce misalignment and ghost effect in the panorama output. The proposed method outperformed the existing methods, namely contrast limited adaptive histogram equalisation (CLAHE) and dark channel prior (DCP). The proposed image enhancement technique has increased contrast, entropy, and colour average by 0.069, 0.43, and 13.96, respectively, than CLAHE, and 0.994, 0.43, and 42.07 than DCP. The accuracy of the object detection model is 97%, and the overall processing time of all the algorithms is 0.44949 seconds.

ARTICLE HISTORY

Received 1 March 2021

Accepted 17 November 2021

KEYWORDS

Foggy weather; driving assistant; video stitching; image processing; object detection; convolution neural network

1. Introduction

The opencast mining sector is vulnerable to significant injuries and fatalities caused due to accidents while working under unfavourable weather conditions like fog, rain, and smog. The fog reduces road tracks' visibility, which leads to a chance of vehicle collision and other major safety issues for the operators driving heavy earth moving machinery (HEMM) at opencast mines [1]. Further, during foggy weather, the opencast mining operation is suspended because of the inability to operate HEMM, which causes substantial loss to the mining industry.

Several research studies have been conducted to overcome the visibility problem during foggy weather during the last two decades. Nieto et al. [2] suggested an assisted driving system (ADS), which helps operators drive vehicles through Google earth's 3D graphics map. Lu et al. [3] presented a technology that provides preliminary information about accidents to the control unit for further potential accidental threats. Sun and Zhang [4] developed a driving assistant system that

CONTACT Sushma Kumari  kumarisushma7870@gmail.com  Sushma Kumari, Room no. - 26, Mine Mechanization, Automation, and Technology Development Group, CSIR-Central Institute of Mining and Fuel Research, Dhanbad 826001, Jharkhand, India., ,

includes a combination of techniques like Google earth, a global positioning system (GPS), a wireless communication network, and an enhanced visibility dashboard for the operator to drive smoothly in an open pit mine. Ruff [5] proposed a method to detect any incoming obstacles using the inbuilt radar-based proximity warning system on the vehicle. Spinneker et al. [6] offered camera-based fast fog detection as an advanced driver assistance system for safe driving during the presence of fog at opencast mines. Hautiere et al. [7] suggested a technology that focuses on detecting fog on the on-board camera using Koschimieder's model hypothesis. Negru and Nedevschi [8] recommended a reliable driving system to detect the drivers' fog and visibility estimation density using an on-board camera. Hautiere and Aubert [9] developed a real-time method for contrast restoration using an on-board camera and the flat world hypothesis. Tan [10] acclaimed visibility restoration of a single image in lousy weather by removing fog from the image while increasing the contrast of the final restored image. Nieto and Dagdelen [11] developed a virtual mine system that incorporates the combined output of GPS, wireless communication network, and 3D mapping of the open pit field for safe driving. Nieto [12] developed real-time proximity and 3D mapping system based on a wireless network. Saurabh et al. [13] introduced different technologies like GPS, dome camera, radar, and Internet of Things (IoT) for mining operations in foggy weather. Chatterjee and Chaulya [14] developed a technique to improve the drivers' visibility through the real-time image enhancement algorithm applied to the on-board vehicle's camera input imagery.

Several studies have been conducted to create the 180° panorama view with proper alignment. The use of contrast-limited adaptive histogram equalisation (CLAHE) for foggy and underwater images with video enhancement has been proposed [15,16]. The mixed image enhancement technique using both CLAHE and discrete wavelet transformations (DWT) has been used for foggy image enhancement [17,18]. Kim et al. [19] have explained a hybrid technique for foggy image enhancement of indoor and outdoor environments. This method includes dark channel prior (DCP) followed by CLAHE and DWT for overall contrast enhancement and virtual histogram stretching of an image. The DCP method estimates atmospheric light's thickness and extracts it for a haze-free image [20–23]. The DCP method gives outstanding results in terms of contrast of an image but destroys its actual colour. Above mentioned approaches only enhance features of the specified portion and some aspects of the image, but it also creates noise and colour distortion.

Tajeen and Zhu [24] created a dataset of construction machines, namely excavator, loader, dozer, backhoe, and roller, to identify the machine's performance in real time. Xiao and Kang [25] developed a deep learning-based object detection model to detect the construction machines and check their status through cameras. The technology helps the project manager to get real-time feedback and alert if any construction machine goes missing.

However, the above technologies' significant drawbacks are that these systems cannot provide a proper real-time vision of the road to HEMM operators in open pit mines and cannot provide multi-stage safety features with warning mechanisms. Thus, there is a requirement for an effective system that can provide an indistinct view of the road and multi-stage safety features to HEMM drivers and operators to continue opencast mining operations during foggy weather and reduce the threat of transportation accidents.

According to Nieto [26], the 5S innovation model is defined as staying competitive and innovative to maintain high growth, productivity, and sustainability levels for any mineral industry. The 5S covers safe, simple, smart, stealth, and sustainable for achieving maximum safety, simplifying systems, using smart-intelligent systems, designing stealth operations, and following a sustainable strategy. The model is designed to be adaptable to any type of mining. Five innovation drivers are defined that are essential for sustainable mining. The model can serve as a road map to develop technologies and the methods for the 'mine of the future'. The paper deals with two 'S' (Smart) and 'S' (Safe) using innovative technologies like artificial intelligence (AI), machine learning, image processing, and embedded sensors and devices.

The Earth Moving Equipment Safety Round Table (EMESRT) [27] has published an updated guideline that provides mining equipment designers interoperability protocols that minimise and reduce vehicle interactions and collisions. The paper deals with the EMESRT guideline for levels 7 and 8. Level 7 states operator awareness using technologies that provide information to enhance the operator ability to observe and understand potential hazards in the vicinity of the equipment. Level 8 explains advisory controls using technologies that provide alarms and instruction to enhance the operator ability to predict a potential unsafe interaction and the corrective action required.

An intelligent driving system for foggy weather in opencast mines has been developed as per the Director-General of Mines Safety (DGMS) guidelines, Government of India [28,29], which has been deployed at Bailadila Iron Ore mines, Chhattisgarh state in India.

This paper proposes a new approach that helps HEMM drivers and operators to drive efficiently without any hindrance caused by fog, dust, and objects. The technology consists of an intelligent system based on real-time image processing and other devices, which helps the operators to drive during those unfavourable weather conditions. The image processing algorithms include real-time image stitching, enhancement, and object detection to combine the output videos of the used 3 cameras installed at the front of the vehicle into an almost 180° panorama view and real-time defogging with the detected obstacles better surveillance. Eventually, the created output video has been deployed in the system through a high-speed graphical processing unit (GPU) for real-time applications. The system integrates hardware and software, and its output is displayed through a dashboard placed in front of the driver's seat. The whole developed system has been installed in different HEMM (i.e. mining loaders, mining trucks, mining shovel machines, mining dozers, mining drill machines, and other mine vehicles). This system helps the drivers to detect the object and provide a clear view of the path. If any other vehicles come nearby, the system generates an alarm so that the driver knows the possible threat of vehicle collision, thus avoiding it and making the system more reliable during adverse weather conditions. The paper presents details of the developed vision enhancement system and algorithms and performance analysis of the image processing algorithms.

2. Methodology

Both hardware and software were integrated to mitigate the problem during adverse weather conditions at the mining site. The system architecture with hardware placement and software algorithms has been discussed further in subsections. Initially, a wireless network was built to connect each vehicle to the control centre for continuous monitoring. At the control centre, the data monitored are Radar feed, vehicle location through GNSS, and all camera output. The whole system provides a comprehensive solution for opencast mines covering the safety levels of 7 and 8 as per the Earth Moving Equipment Safety Round Table (EMESRT) guidelines [27]. The details of all the hardware and software have been given in [Table 1](#).

2.1. System architecture

[Figures 1 and 2](#) show the developed system architecture for installing mining dump truck and mining shovel machine, respectively, working in an opencast mine. The whole system consists of a framework of hardware and software. The hardware includes (a) Internet protocol (IP) thermal and high definition cameras, (b) global navigation satellite system (GNSS), (c) proximity radar, (d) anti-collision laser light, (e) wireless device, (f) graphical processing unit (GPU), (g) touch screen, (h) retro-reflecting material, (i) network switch and other roadside edge detection devices like a flashlight, self-regulating heating cable, LED lights and retro-reflecting material as well as LED-fitted vests, and thermal binoculars are provided to field supervisors for better visibility through the

Table 1. Details of hardware and software of the proposed system.

Type of hardware/software	Solution	Level of safety as per EMESRT [27]	DGMS guidelines
Hardware:			
• IP camera	For monitoring the front and rear view of the vehicles. It is also used for creating panorama and image enhancement algorithm	Level-7	DGMS (Tech) Circular No. 6, 2020. All cameras should be as per ISO 16001 and ingress protection of IP69K [28]
• Proximity radar	To detect and generate the alarm if any obstacle is found in the range of 50 m	Level-8	DGMS (Tech) Circular No. 6, 2020 [28]
• GNSS module	To provide the real-time location for each vehicle with higher accuracy of less than 10 cm	Level-8	DGMS (Tech) Circular (MAMID) No. 8, 2020 [29]
• Anti-collision laser light	It is fitted on the rear side of the vehicle to indicate a safe distance while reserving the vehicle	Level-8	-
• Self-regulating heating cable	To be laid down on edges of the road so that it can be detected through thermal camera to mark the road edge	Level-7	-
• Rugged GPU processor	It is the processing unit that collects data from all the devices and sensors for processing	Level-7	-
• Touch screen display	It is used to display the output of all algorithms to the operator	Level-7	-
• Wireless devices and network switches	They are used to create a wireless network so that all the vehicles are connected for information exchange	Level-7	-
• Retro-reflective material	They have been used to indicate the upcoming vehicle if light falls on the materials	Level-7	-
Software:			
• Real-time image stitching	It takes three front camera inputs and stitches them together to get a 180° panorama view	Level-7	-
• Real-time image enhancement	It takes real-time foggy images and enhances them to get a clear view	Level-7	-
• GNSS-based proximity awareness	Takes input from GNSS and create alarm at the range of 25 m	Level-8	-
• Radar-based proximity warning	Takes input from radar and create alarm up to the detection range of 50 m	Level-8	-
• Vehicle tracking software	It used GNSS live location for tracking each vehicle present in the mine site	Level-7	-
• Navigation using 3D geo-tagged mine map	Through the software, the live location of any vehicle is displayed on a 3-D map of the mine	Level-8	-
• Fleet management software:	This software contains multiple features like:	Level-7	-
• Production monitoring	It is used to monitor the daily production of the mines	Level-7	-
• Geofencing	Geofencing of the mine is created virtually to monitor the mineral loaded truck to prevent mineral theft	Level-7	-
• Optimisation mining loaders and dump trucks performance	It continuously monitors the performance of mining loaders and dumps trucks by reducing the idle time	Level-7	-
• Trip count	It counts the loading and unloading trips of the mining trucks	Level-7	-

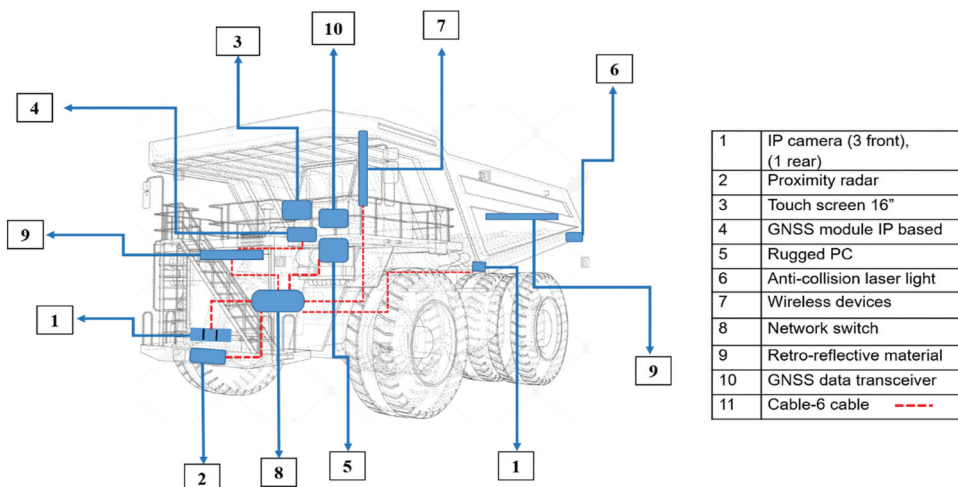


Figure 1. The system architecture for the mining dump truck (Source: www.shutterstock.com).

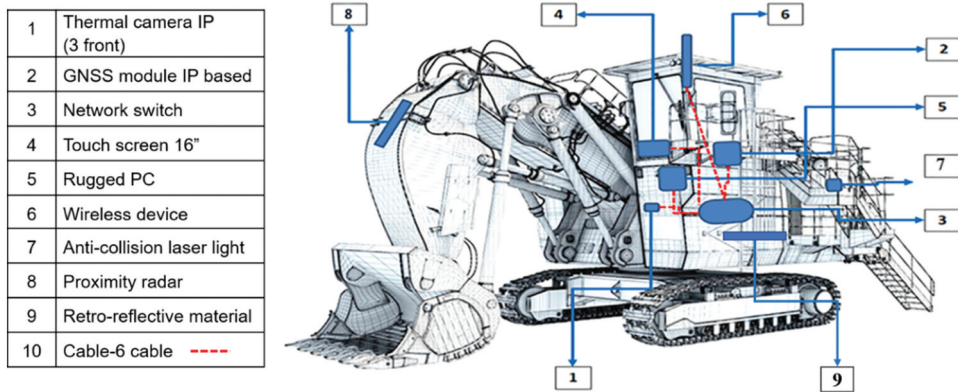


Figure 2. The system architecture for a mining shovel machine (Source: www.shutterstock.com).

thermal camera during foggy weather. The software includes integrated image processing algorithms, GNSS software, and proximity warning algorithms deployed in a high-speed GPU for its real-time functions.

Three IP cameras are installed in the front to cover the entire width of the mining truck (dumper) and provide a 180° view of the front road, and a rear camera offers a rear view of the road to the operator when operating a HEMM in an opencast mine. As the field of view of one camera is insufficient to cover the wanted area, three cameras have been used to cover the whole front area of the mining truck, as depicted in Figure 3. The image stitching technique has been used to combine three output videos of the cameras with their common field of view to create the segmented panorama video. The camera's input image first goes through the integrated algorithm, and the final output is displayed on the dashboard screen fitted on the front of the driver seat. The final processed image can provide a dehazed image and detect any obstructions on the operator's path with its wide field of view.

A GNSS module is installed on the vehicle's front to locate its accurate position and other vehicles around it on the mine map. It also performs different functions of vehicle tracking and fleet management, which: (i) provides real-time monitoring and displays all vehicle's locations on Google or mine map; (ii) calculates the distance from the nearest vehicle and provides proximity

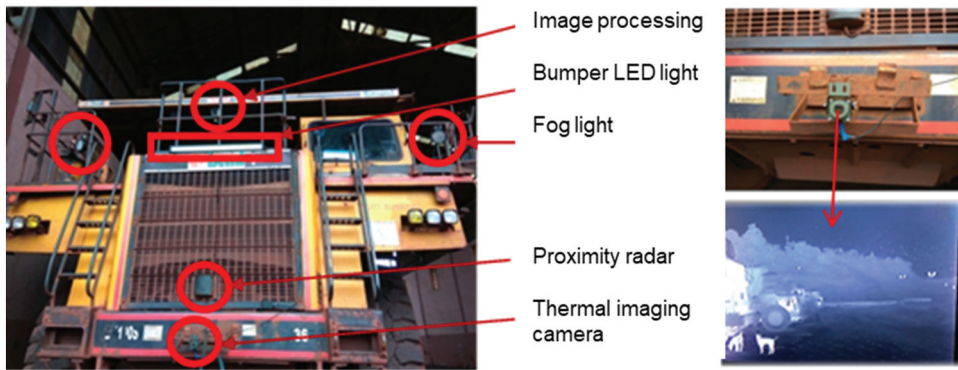


Figure 3. Architecture of the system deployed in the field.

warning when approaches within the specified safe distance; (iii) displays and reports of total run time, total distance travelled, number of trips, time is taken between stops and during a trip, stoppage reports with round trips travelled by the vehicle, path history, geofence area deviations, etc.; (iv) provide notification alerts when GNSS unit is tampered or cut off from the vehicle battery, route violation, geofence violation, stoppage beyond specific period; and (v) incorporates fleet management facility for optimisation of shovel-dumpers performance. The GNSS data transceiver transmits vehicle position to the nearest base station and simultaneously receives other vehicles' position inside mine premises onto its dashboard screen.

Apart from this, a proximity radar is also installed on the front side of the vehicle having a detection range of 50 m. A proximity warning device has the following features:

- Detects static and moving objects, including human beings, on its own during the vehicle movement for a specified range and warn the operator;
- Provides an adjustable audio-visual warning when it detects static and moving objects, including human beings, least height light motor vehicle used in the mine, etc., within the virtual target area of respective dumper/truck;
- The width of the virtual target area is equal to the width of the dumper/truck plus 0.5 m on both sides;
- The centreline of the virtual target area coincides with the dumper/truck centreline;
- Length of the virtual target is around 50 m or adjusted equal to the extent of dumper/truck; and
- The system has intelligent alert generating mechanisms to indicate an obstacle in the vehicle's pathway, whether left, right, or centre, triggering audio alerts after detecting obstacles. The alert is an auto-cut off type to avoid operator inconvenience/distraction.

The system has the provisions for recording video footage and details of a warning generated with a timestamp to enable easy retrieval and analysis of the immediate past 96 deployment operating hours. The IP camera's processed output, proximity radar, and GNSS module have been integrated on a 16-inch touchscreen display board mounted on the driver seat's front. The display board is further split into 4 windows to represent each independent function, as shown in **Figure 4**.

The top half displays the output of integrated algorithms applied to IP cameras; the lower section is further divided into three windows for proximity radar view, GNSS module output, and the road's rear-view for other safety purposes. The drivers can select any particular window using a touch panel to display on full screen. In contrast, the other windows continue to run in the background and pop up an alert when necessary. A network switch is used for the terminal

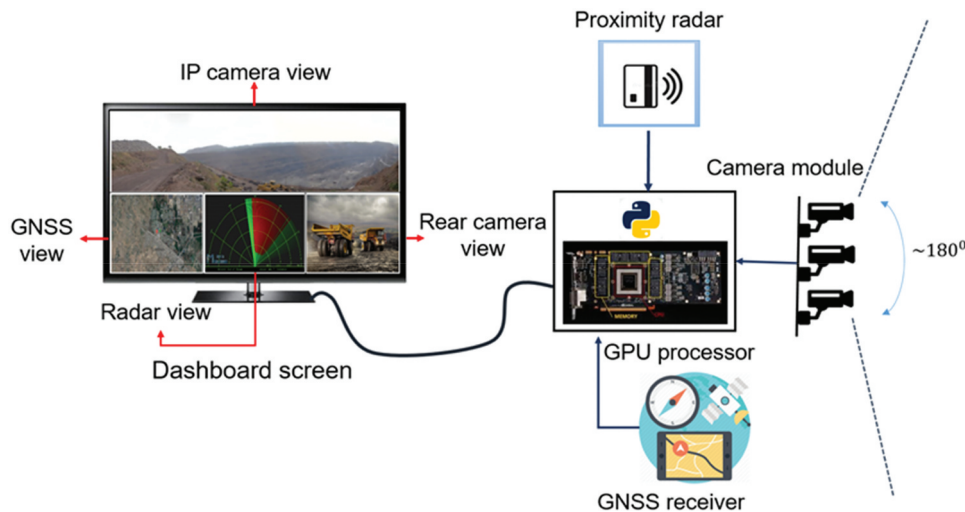


Figure 4. Installation layout of three cameras, GNSS and proximity radar, and display unit.

connection of all Ethernet-based modules such as cameras, proximity radar, and GNSS. Finally, a rugged PC is used to process all the cameras, proximity radar, and GNSS information. The power required to run the whole system is derived from the vehicle only.

In addition to the above equipment, some other devices are also incorporated in the system, like retro-reflective material, LED-fitted vest, anti-collision laser light, and flasher light. Retro-reflective material is primarily used to increase the night-time conspicuity of traffic signs, road surfaces, road signs, vehicles, etc. The LED-fitted vest is used for field personnel to make them effectively visible through the camera. Anti-collision laser light is installed on the vehicle's rear end to warn the other operator behind it and avoid traffic accidents while driving in the rain, fog, and low light conditions. Further, self-regulating heating cables and LED strips are laid on some parts of road edges to properly detect the operators' sharp turns while driving HEMM during foggy weather conditions. The developed system enhances the operators' visibility. It provides a better module by generating an alert mode as a safety measure to avoid any further threat of vehicle collision during foggy weather conditions. Besides this, the system also covers other safety parameters to take further precautions when the climatic conditions are not favourable for mining, such as foggy weather.

2.2. System software algorithm

Figure 5 shows the algorithm of the developed system. The input frame is taken by the 3 individual cameras connected to the GPU processor (NVIDIA TX2). The camera's power supply is connected to the vehicle powertrain to initialise. The GPU continuously checks whether the cameras are in 'on' or 'off' mode. If the cameras are 'on', then only it takes the inputs for next-level processing. The GPU processor is deployed with the three video processing algorithms, namely (i) real-time image stitching, (ii) image enhancement, and (iii) object detection. All the algorithms take the input from cameras and process it for the final output, displayed on a dashboard screen for the HEMM operator.

2.2.1. Real-time image stitching

The algorithm for real-time image stitching is depicted in Figure 6. The significant steps involved for image stitching are colour transfer, feature points detection, sorting of good feature points, feature point matching, warp perspective transforms for stitching, etc.

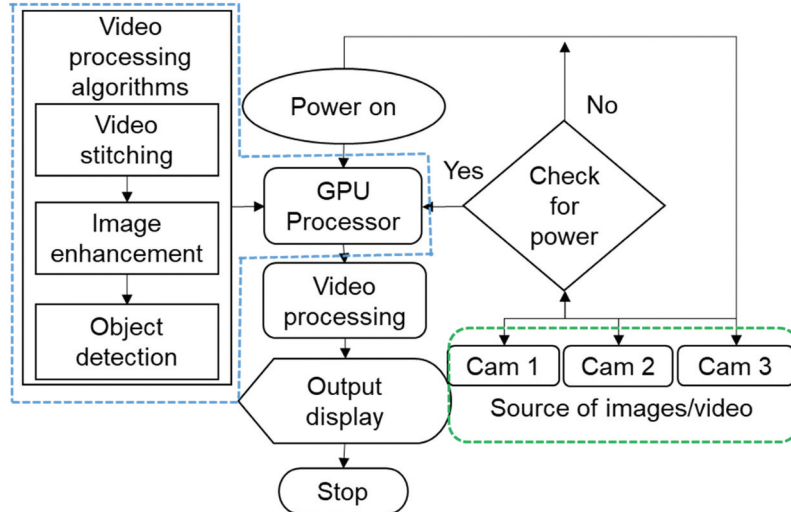


Figure 5. Developed system algorithm.

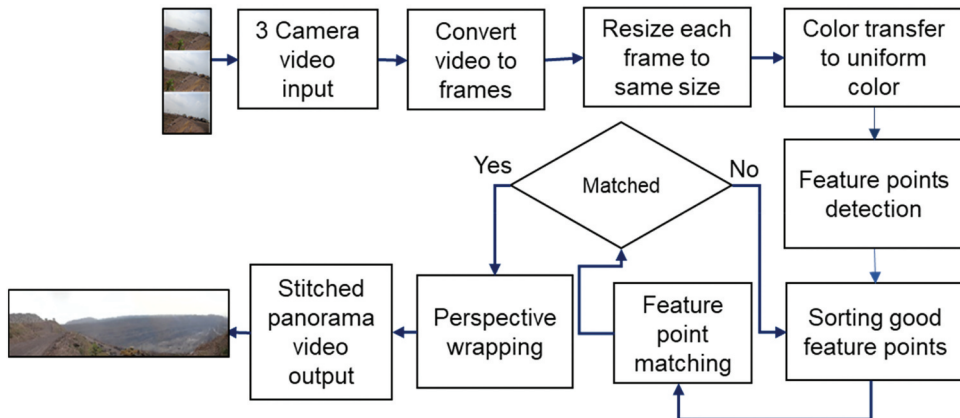


Figure 6. Real-time image stitching algorithm for taking input of three individual cameras and constructing a 180° panorama view.

2.2.1.1. Colour transfer. Due to the colour inconsistency between the frames, it is difficult and time-consuming to match the stitching feature points. Colour transfer is a technique in which one frame's colour element is transferred to others to make them even tone. LAB colour space has been used for the colour transfer of the target image [30]. The steps involved in the colour transfer are as follows:

- Split the colour space of both the target and source images;
- Determine the mean and standard deviation of each channel; and
- Subtract the mean from the target image using the following equations:

$$l = l - \bar{l}_t \quad (1)$$

$$\alpha = \alpha + \bar{\alpha}_t \quad (2)$$

$$\beta = \beta + \bar{\beta}_t \quad (3)$$

- Scale by the standard deviations using:

$$l = (\sigma l_t / \sigma l_s) * l \quad (4)$$

$$\alpha = (\sigma \alpha_t / \sigma \alpha_s) * \sigma \quad (5)$$

$$\beta = (\sigma \beta_t / \sigma \beta_s) * \beta \quad (6)$$

- Add the mean of the source image by applying:

$$l = l + \bar{l}_s \quad (7)$$

$$\alpha = \alpha + \bar{\alpha}_s \quad (8)$$

$$\beta = \beta + \bar{\beta}_s \quad (9)$$

Where l is lightness (intensity), α is a colour component ranging from green to magenta, β is a colour component ranging from blue to yellow, l_t is the mean of lightness, α_t is the mean of colour component ranging from green to magenta, β_t is the mean of colour component ranging from blue to yellow for the target image, l_s is the mean of lightness, α_s is the mean of colour component ranging from green to magenta, and β_s is the mean of colour component ranging from blue to yellow for the source.

2.2.1.2. Feature points detection. Feature points of an image are invariant points under lightning conditions, zoom, and view change. The scale-invariant feature transform (SIFT) method has been used to detect feature points. The key points are invariant to image rotation and scale, which is robust across a substantial range of affine distortion, the addition of noise, and change in illumination [19]. OpenCV library has been used to access the SIFT function for feature detection.

2.2.1.3. Sorting of good feature points. Feature points that have the shortest distance are considered good feature points for matching. The shortest distance between the points of two consecutive frames is calculated using Euclidean distances. According to Anton [31], in the Euclidean plane (Figure 7), if $p = (p_1, p_2)$ and $q = (q_1, q_2)$, then the distance is given by.

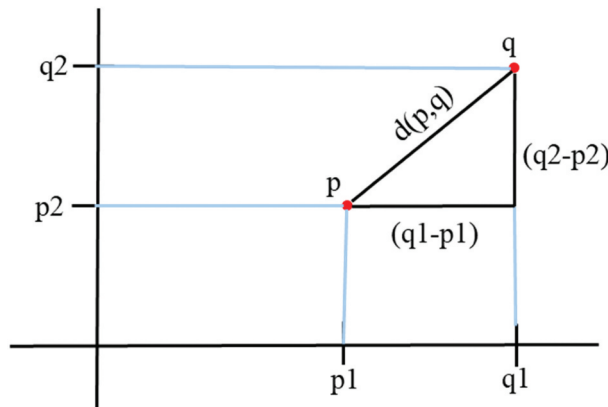


Figure 7. Euclidean distance calculation where p and q are two points on the same plane.

$$d(p, q) = \sqrt{(q_1 - p_1)^2 + (q_2 - p_2)^2} \quad (10)$$

It is similar to the Pythagorean theorem [31].

2.2.1.4. Feature point matching. After getting good feature points on both images, the homography matrix is estimated. The homography is the 3×3 transformation matrix, which maps the points on an image to the corresponding point in another image [32]. Let (x_1, y_1) is the corresponding point on the first image to the point (x_2, y_2) on the second image, then the transformation is given by:

$$(x_1, y_1) = H(x_2, y_2) \quad (11)$$

Where H is a homography matrix which is given by:

$$H = \begin{bmatrix} h_{00} & h_{01} & h_{02} \\ h_{10} & h_{11} & h_{12} \\ h_{20} & h_{21} & h_{22} \end{bmatrix}$$

Now, the equation can be written as:

$$\begin{bmatrix} x_1 \\ y_1 \\ 1 \end{bmatrix} = \begin{bmatrix} h_{00} & h_{01} & h_{02} \\ h_{10} & h_{11} & h_{12} \\ h_{20} & h_{21} & h_{22} \end{bmatrix} \begin{bmatrix} x_2 \\ y_2 \\ 1 \end{bmatrix} \quad (12)$$

The Brute-Force matcher has been used, which takes the descriptor of one feature in the first set and matches all other features in the second set of images. The inbuilt function of OpenCV for Brute force matching has been used in the python scripting language. An example of a keypoint feature matching image is illustrated in Figure 8.

2.2.1.5. Warp perspective transforms for stitching. This process is used for the geometrical transformation of the source image. It does not change the content of the image but deforms the pixel grids. It deforms the source image's pixel grid (train image) according to the query image to form a destination image with the following function [33]:

$$dst(x, y) = src\left(\frac{M_{11x} + M_{12y} + M_{13}}{M_{31x} + M_{32y} + M_{33}}, \frac{M_{21x} + M_{22y} + M_{23}}{M_{31x} + M_{32y} + M_{33}}\right) \quad (13)$$



Figure 8. Key point feature matching process, where each pair of a common point is matched and displayed with different colour lines.

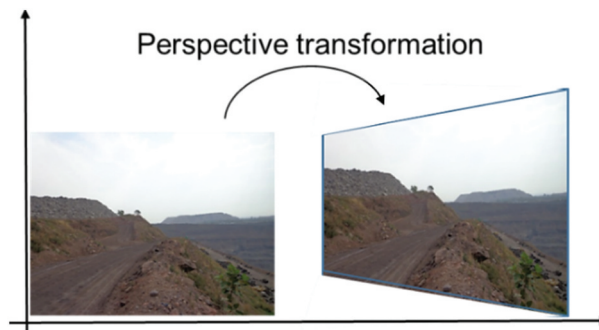


Figure 9. Image perspective warp transformation process.

$dst(x, y)$ is the destination image, src is the source image, and M is the transformation matrix. The process of perspective warp transformation is depicted in Figure 9.

2.2.2. Real-time image enhancement

A foggy image is generated due to scattering source light through the atmosphere without reaching the target object. The presence of fog in the image mainly affects the image's contrast, sharpness, and true colour. A real-time image enhancement method has been proposed to enhance the image's visibility, which is presented in Figure 10.

Red, green and blue (RGB) channels of the foggy image are converted to hue, saturation, and value (HSV) channel and then split into the individual channel so that the CLAHE filter can apply to the value (V) channel. Again the HSV merges back and reverses converted into an RGB channel. CLAHE stretches the histogram of foggy images into an entire span of 0 to 255, limiting the occurrence frequency of grey levels. A high pass filter has been used for sharpening the image to rectify the blurriness in the images. All these artificial processing can damage the images' actual colour; hence, a colour correction method has been used to persist the image's actual colour. All these processes have been done in real-time in a fraction of a second. The processed final output is then fed to the object detection algorithm as an input further.

The proposed method is called CLAHE with image sharpening and colour correction (CISACC). The CISACC method is also compared with the existing normal CLAHE and DCP methods.

2.2.3. Real-time object detection

During foggy weather, the recognition of any person or vehicle in surrounding areas becomes difficult for the operators while driving HEMM, which leads to a significant threat of accidental injuries due to collision. This paper proposes a real-time implementation of object detection using a convolution neural network (CNN) at opencast mines to facilitate accurate tracking and recognition of vehicles and workers during mining operations.

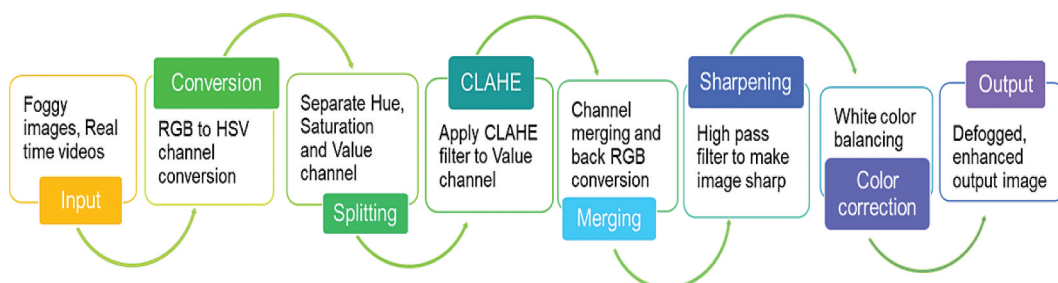


Figure 10. Block diagram for the real-time image enhancement process.

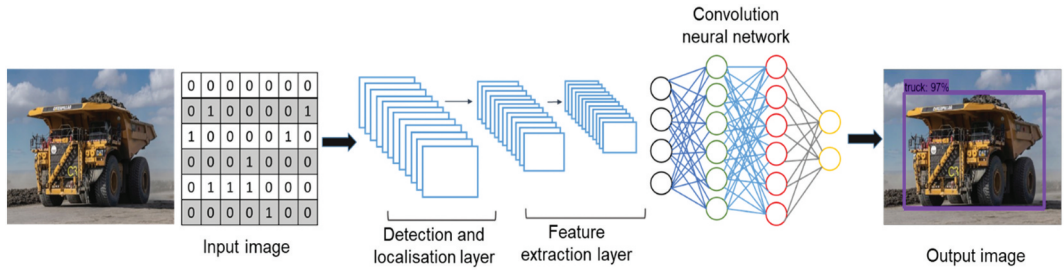


Figure 11. The work function of object detection using CNN.

Table 2. Details of data splitting, where the total number of training images for each class is given with their source.

Class	Total images	Data source
Truck	694	ImageNet [34]
Excavator	681	ImageNet, Kaggle [39]
Jeep	795	ImageNet
Drill machine	692	ImageNet
Person	794	ImageNet

The whole workflow of developing the CNN-based obstruction detection is based on two phases, i.e. dataset preparation and training the final model (Figure 11). Several images from all environmental conditions were collected using the ImageNet dataset community for building datasets [34]. Moreover, in other image search engine platforms, around 4700 images were extracted, and an input image was resized (800×600 dimensions) and labelled manually to build this dataset, which contains classes of different mining machinery, like mining truck (dumper), jeep, drill machine, excavator, dragline, etc. (Table 2). The final dataset has been trained on a single shot detector (SSD)-MobileNet architecture model known for its excellent performance with speed and fair accuracy. It uses machine learning platforms, like TensorFlow and OpenCV [35–38]. For training, the dataset was split into 80% for training purposes and 20% for testing purposes, and this training set was further divided into 80% for training purposes, and the remaining 20% of the data was used for validation purposes. Firstly, the image stream captured from cameras was put into the SSD-MobileNet model in real-time; the model was further trained according to the defined dataset where the detected images with bounding box coordinates (x, y) of each object were shown to the operator through a dashboard screen for proper visualisation (Figure 11). The methodological overview of the object detection algorithm is shown in Figure 12.

3. Results and discussion

3.1. Image stitching

Several pairs of images have been tested and evaluated to create panorama images to represent the proposed algorithm's effectiveness. Some of the images were taken from mines and buildings, which are presented in Figures 13 and 14, respectively. Figure 13(a) shows the output image of three IP cameras installed in front of the vehicle. Figure 13(b) shows its respective output image, which is displayed as a panorama view in the dashboard screen placed in front of the driver's seat. This system provides the driver a 180° field of view to minimise accidental threats and continue mining without any hindrance. Similarly, the three individual cameras' output is shown in Figure 14(a), and their respective panorama view is illustrated in Figure 14(b) for a building area.

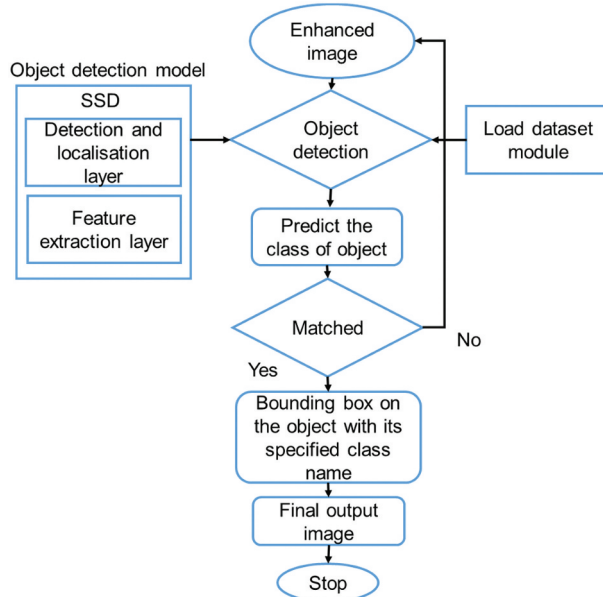


Figure 12. Flowchart of the object detection algorithm.

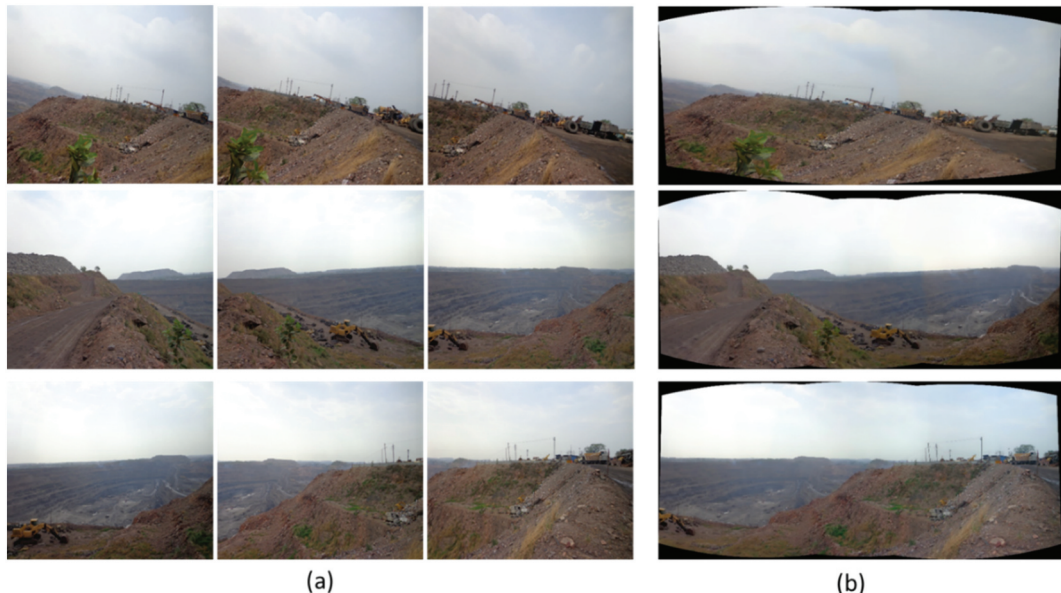


Figure 13. Mining site output image: (a) three-camera individual output, and (b) final panorama output.

Intensity inconsistency in the stitching frames creates low match points detection and false keypoint matching, which may generate ghost effects and misalignment in the panorama output. Hence, the colour transfer method has been used before stitching the images for better blending and stable keypoint matching. The visual assessment has been carried out to quantify colour and transfer in the image stitching algorithm. Figure 15(a), (c), and (e) shows the panorama image without colour transfer where the ghost effect has been presented in the yellow boxes. In contrast, red boxes represent the misalignment of features.

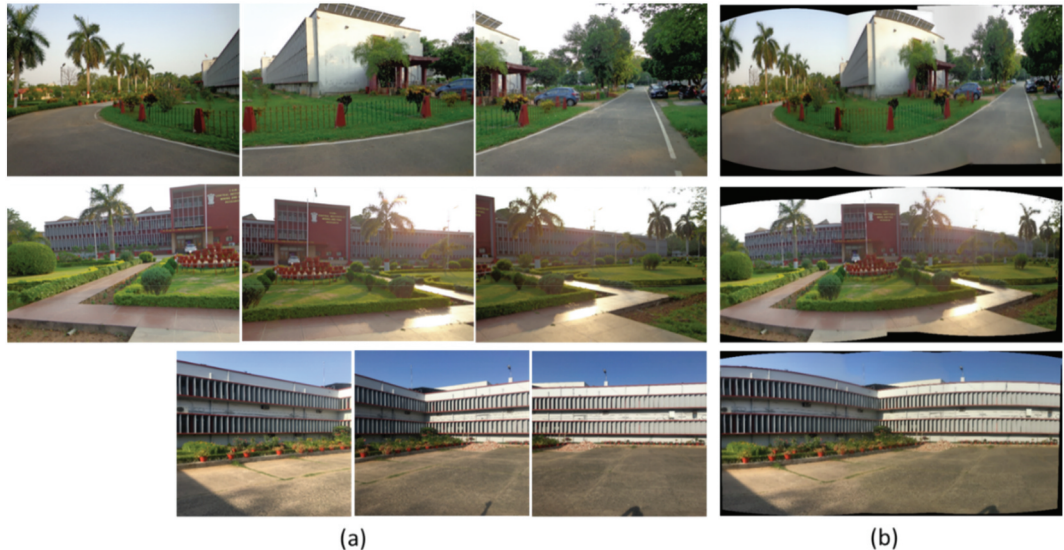


Figure 14. Building site output image: (a) three-camera individual output, and (b) final panorama output.

Figure 15(b), (d), and (f) shows the corrected panorama image with colour transfer method, and its respective rectified output has been illustrated in the boxes. Thus, the proposed algorithm has a more refined output in comparison to the standard panorama view.

3.2. Image enhancement

The proposed algorithm has been compared with the existing two defogging methods, i.e. normal CLAHE and DCP methods. Three images have been used as testing images, and resultant processed images are shown in Figure 16, whereas Figure 16(a-e) illustrate original image of opencast mines without fog, original image of opencast mines in foggy condition, standard CLAHE image, DCP image, and CISACC processed image, respectively. It has been observed that the CISACC processed image has better visibility than the other two methods. However, the output image by the CISACC algorithm has lesser visibility than the image without fog. As the mining activities are dynamic, the mine site situation was not the same while taking images with and without fog at different times. Hence, there is a small variation in images with and without fog conditions.

The image processing performance of all the methods was assessed and compared using various parameters like contrast, entropy, colour average, mean squared error (MSE), and peak signal-to-noise ratio (PSNR) are summarised in Table 3. It has been evaluated that the proposed CISACC algorithm has increased contrast, entropy, and colour average by 0.069, 0.43, and 13.96 respectively than the normal CLAHE, and 0.994, 0.43, and 42.07 respectively than the DCP processed image. Figure 17 shows that the CISACC method has higher contrast, entropy, and colour average than the other two methods. The mean square error of CISACC is slightly lower than both methods, and PSNR is almost equal to 30 dB, which indicates better performance [40].

Processing time is the time required by the algorithm to process the image. The image enhancement algorithm's processing speed has been tested using six test images of the same resolution (4408×3456). The processing time has been calculated and compared for all three methods (Table 4).

The CISACC method combines CLAHE with sharpening and image colour correction. Still, its processing speed is almost the same as normal CLAHE, and it takes 0.52 second less processing time than DCP, which is graphically represented in Figure 18.

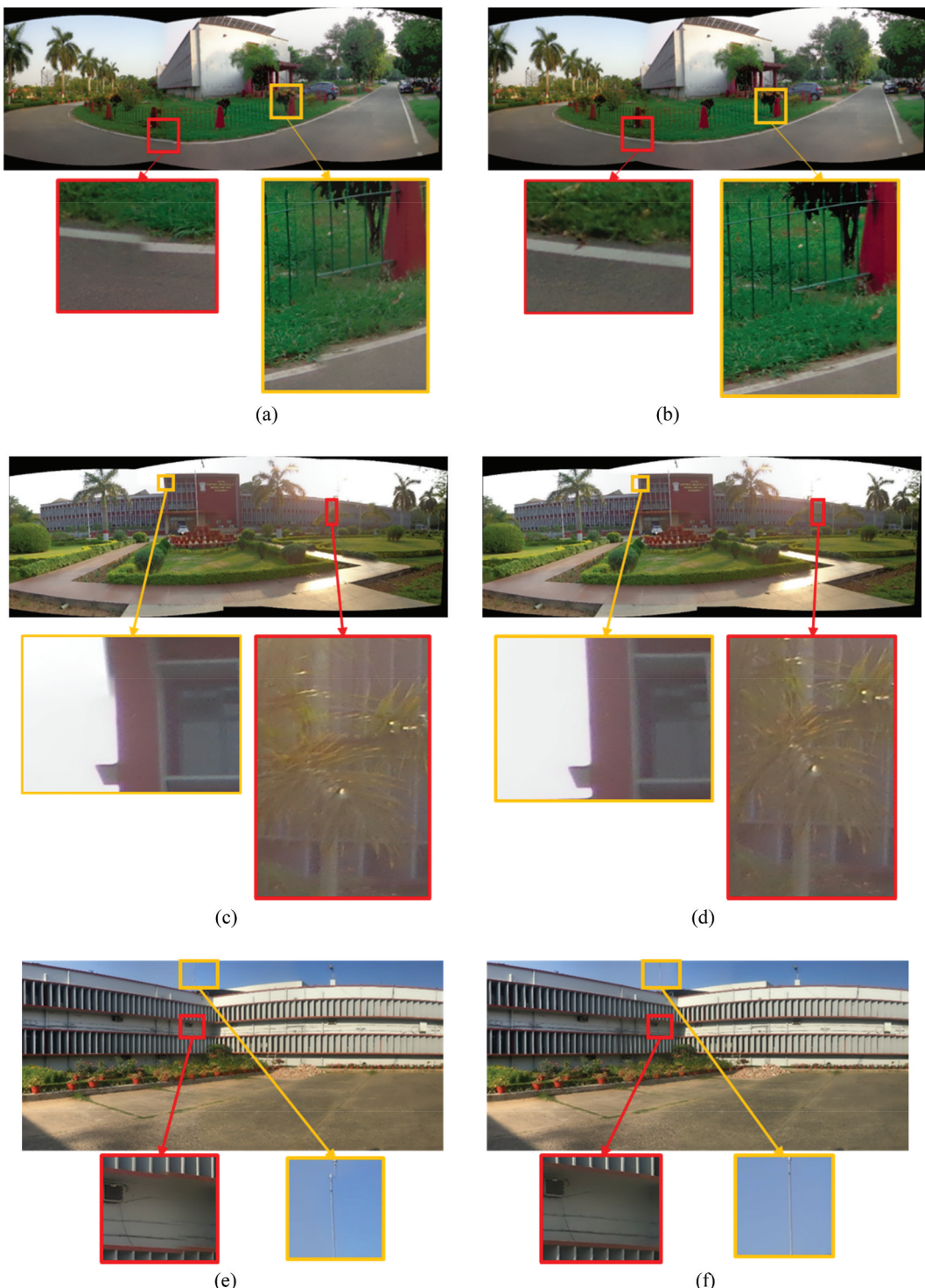


Figure 15. Error comparison: (a), (c) and (e) stitched image without colour transfer; and (b) (d) and (f) stitched image with colour transfer.

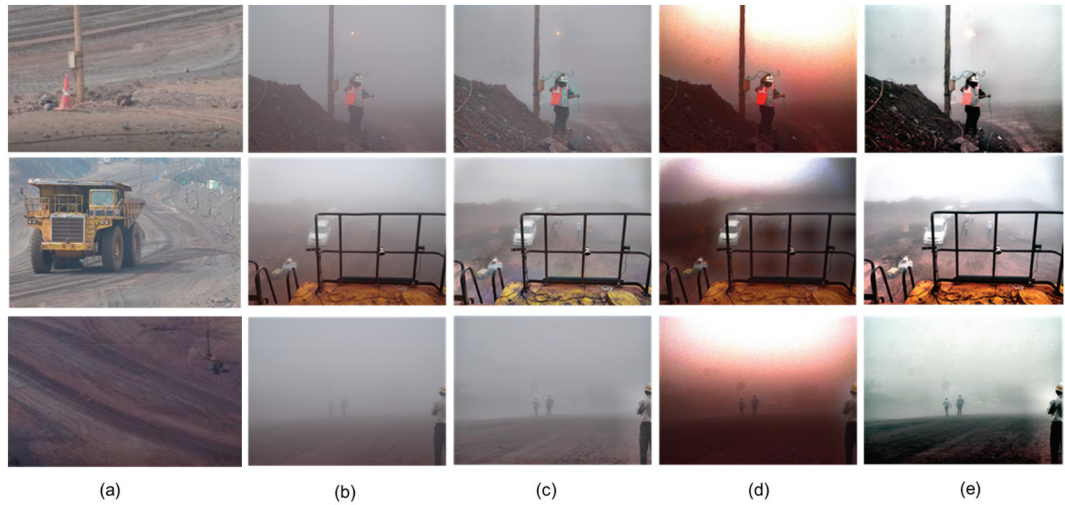


Figure 16. Enhancement results: (a) original image of opencast mines without fog, (b) original image of opencast mines in foggy condition (c) standard CLAHE output, (d) DCP output, and (e) CISACC output.

Table 3. Performance evaluation using various parameters for different image processing algorithms.

Image	Method	Contrast	Entropy	Mean	PSNR	Colour average	Keypoint
Miner with pole	Original image	0.253	5.4			140.61	21
	CLAHE	0.166	6	35.99	27.62	141.32	284
	DCP	0.016	6	104.41	27.94	127.84	160
	CISACC	1	6.4	112.39	32.56	152.31	1190
Vehicles	Original image	1.518	5.4			143.35	7
	CLAHE	1.29	5.5	32.13	27.66	144.94	64
	DCP	0.004	5.5	117.44	27.43	124.81	15
	CISACC	1	6.2	111.4	33.06	156.027	269
Miners	Original image	1.022	6			140.811	439
	CLAHE	1.084	6	78.49	27.58	148.06	856
	DCP	0	6	112.97	27.6	97.341	388
	CISACC	1	6.2	113.43	29.18	167.87	1053
Average	Original image	0.931	5.6			141.59	155.67
	CLAHE	0.845	5.83	48.87	27.62	144.77	401.33
	DCP	0.006	5.83	111.60	27.65	116.66	187.66
	CISACC	1	6.26	112.40	31.60	158.73	837.33

3.3. Object detection

To evaluate the detection model's performance, around 50 test images have been collected from opencast mines to determine the class of the selected object in the image by outputting the bounding box around it. Some of its final output results are shown in Figure 19.

The accuracy has been calculated using the K-fold cross-validation method for 100 epochs [41]. Figure 20(a) shows the graphical representation of the gained model accuracy/loss. In contrast, Figure 20(b) depicts the training process that has been done through a high-speed GPU processor, and finally, the graph has been plotted with a training accuracy of 97%. The result represents that the algorithm has been succeeded in real-time implementation at opencast mines.

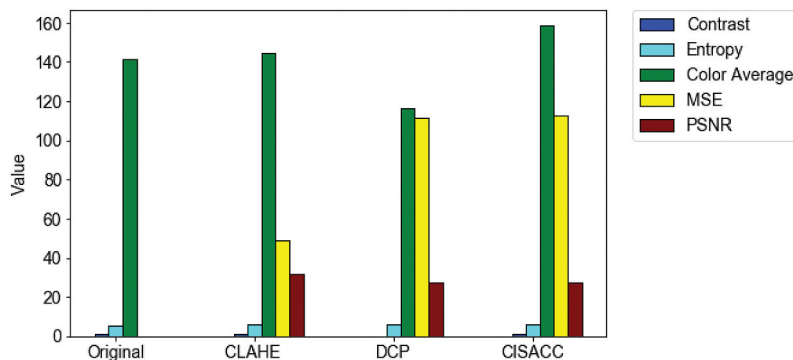


Figure 17. Performance evaluation of different image processing algorithms, where the x-axis shows the different algorithms for image enhancement and the y-axis shows the normalised value of each parameter.

Table 4. Image enhancement time of different methods for various types of images.

Image type	Time (second)		
	CLAHE	DCP	CISACC
Miner with pole	0.045	0.597	0.106
Vehicle	0.057	0.621	0.098
Miner	0.059	0.598	0.097
Electric pole	0.065	0.603	0.097
Road	0.061	0.602	0.094
Truck	0.073	0.635	0.097
Average	0.06	0.61	0.09
Std. Dev.	0.009	0.015	0.004

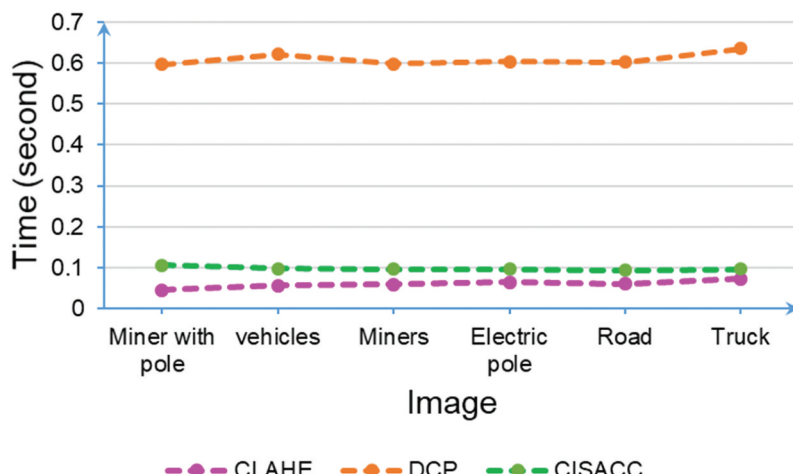


Figure 18. Image enhancement time for different images, where the x-axis is different tested foggy images, and the y-axis shows the time taken in seconds.



Figure 19. Object detection with a bounding box and accuracy.

3.4. Processing time for all algorithms

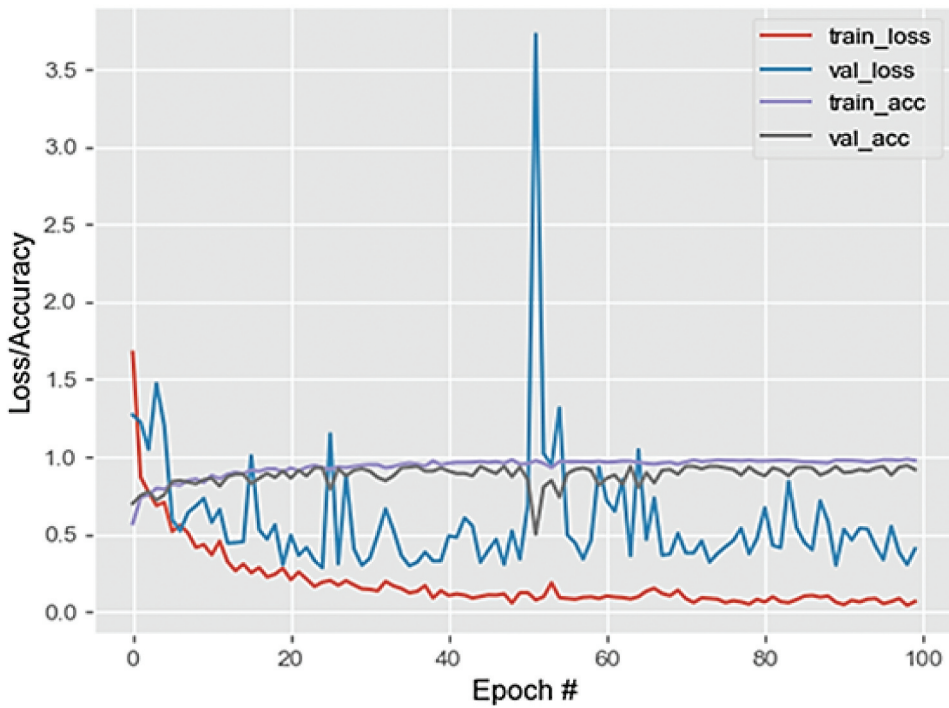
All the proposed algorithms have been integrated and deployed on the NVIDIA GPU processor. The algorithm's execution pipeline is divided into GPU and CPU for parallel processing. Execution time taken by GPU and CPU is 0.05051 and 0.05906 second, respectively. The time for capturing the first frame is 0.07549 second, and the delay or lost time is 0.26443 second. The total time taken for the execution of the whole algorithm is 0.44949 second ([Figure 21](#)).

For further evaluation, the GPU power consumption has been calculated with and without applying image processing algorithms with voltage supplied of 19 V. The initial power consumption was 6.327 W, and the final power consumption was 12.958 W while using the image processing algorithms.

4. Conclusions

The developed technology includes integrating both hardware and software to restore the mining operation during unfavourable environmental conditions. The developed system consists of real-time image processing and the latest technologies like thermal and HD cameras, GNSS, radar, etc., providing better driving conditions and safety features for HEMM drivers and operators during adverse weather conditions. The image processing unit mainly contains three algorithms: image stitching, image enhancement, and object detection. All the algorithms have been assessed for their accuracy, performance, and optimisation. The real-time image stitching method has been used to stitch the three-camera output together to create a wide field of view of 180°. The methodology used for the panorama view has been assessed and compared with and without colour transfer methods. It has been found that the proposed technique outperforms the stitching method without colour transfer in terms of blending, alignment, and ghost effect for creating a panorama view.

For enhancing the image, the CISACC method has been used and compared with the existing normal CLAHE and DCP methods. It has also been evaluated that the proposed CISACC algorithm has increased contrast, entropy, and colour average by 0.069, 0.43, and 13.96 respectively than the usual CLAHE method and 0.994, 0.43, and 42.07 respectively than DCP processed image. Further, the CISACC method takes 0.52 second less processing time than the DCP method.



(a)

```

Epoch 86/100
24/24 [=====] - 50s 2s/step - loss: 0.0857 - acc: 0.9661 - val_loss: 0.7025 - val_acc: 0.8316
Epoch 87/100
24/24 [=====] - 50s 2s/step - loss: 0.0785 - acc: 0.9778 - val_loss: 0.4687 - val_acc: 0.8878
Epoch 88/100
24/24 [=====] - 50s 2s/step - loss: 0.0567 - acc: 0.9786 - val_loss: 0.3450 - val_acc: 0.9439
Epoch 89/100
24/24 [=====] - 49s 2s/step - loss: 0.0756 - acc: 0.9700 - val_loss: 0.2966 - val_acc: 0.9286
Epoch 90/100
24/24 [=====] - 49s 2s/step - loss: 0.0799 - acc: 0.9713 - val_loss: 0.2573 - val_acc: 0.9388
Epoch 91/100
24/24 [=====] - 50s 2s/step - loss: 0.0959 - acc: 0.9739 - val_loss: 0.3122 - val_acc: 0.9337
Epoch 92/100
24/24 [=====] - 49s 2s/step - loss: 0.1177 - acc: 0.9638 - val_loss: 0.2965 - val_acc: 0.9388
Epoch 93/100
24/24 [=====] - 56s 2s/step - loss: 0.0823 - acc: 0.9682 - val_loss: 0.2829 - val_acc: 0.9286
Epoch 94/100
24/24 [=====] - 52s 2s/step - loss: 0.0897 - acc: 0.9682 - val_loss: 0.7194 - val_acc: 0.8776
Epoch 95/100
24/24 [=====] - 51s 2s/step - loss: 0.1094 - acc: 0.9713 - val_loss: 0.8442 - val_acc: 0.8571
Epoch 96/100
24/24 [=====] - 50s 2s/step - loss: 0.0520 - acc: 0.9870 - val_loss: 0.4529 - val_acc: 0.9184
Epoch 97/100
24/24 [=====] - 50s 2s/step - loss: 0.0973 - acc: 0.9661 - val_loss: 0.8716 - val_acc: 0.8673
Epoch 98/100
24/24 [=====] - 50s 2s/step - loss: 0.0980 - acc: 0.9687 - val_loss: 0.5877 - val_acc: 0.8980
Epoch 99/100
24/24 [=====] - 50s 2s/step - loss: 0.0828 - acc: 0.9818 - val_loss: 0.4747 - val_acc: 0.8980
Epoch 100/100
24/24 [=====] - 50s 2s/step - loss: 0.0828 - acc: 0.9700 - val_loss: 0.4494 - val_acc: 0.8929

```

(b)

Figure 20. Accuracy calculation: (a) accuracy/loss graph of the object detection model, and (b) training process output with 100 epochs.

total: 0.44370	cap: 0.07538	worker: 0.05386	gpu: 0.05386	cpu: 0.05848	lost: 0.25598
total: 0.45499	cap: 0.07712	worker: 0.05456	gpu: 0.05456	cpu: 0.06000	lost: 0.26331
total: 0.45028	cap: 0.07651	worker: 0.05113	gpu: 0.05113	cpu: 0.05539	lost: 0.26725
total: 0.45531	cap: 0.07721	worker: 0.05166	gpu: 0.05166	cpu: 0.06146	lost: 0.26497
total: 0.44594	cap: 0.07489	worker: 0.05135	gpu: 0.05135	cpu: 0.05712	lost: 0.26258
total: 0.44988	cap: 0.07549	worker: 0.05133	gpu: 0.05133	cpu: 0.06047	lost: 0.26259
total: 0.45781	cap: 0.07621	worker: 0.05106	gpu: 0.05106	cpu: 0.06267	lost: 0.26787
total: 0.44998	cap: 0.07611	worker: 0.05573	gpu: 0.05573	cpu: 0.05855	lost: 0.25959
total: 0.46362	cap: 0.07729	worker: 0.04872	gpu: 0.04872	cpu: 0.05936	lost: 0.27824
total: 0.44590	cap: 0.07553	worker: 0.05230	gpu: 0.05230	cpu: 0.05792	lost: 0.26016
total: 0.44672	cap: 0.07508	worker: 0.05183	gpu: 0.05183	cpu: 0.06425	lost: 0.25556
total: 0.43168	cap: 0.07208	worker: 0.05147	gpu: 0.05147	cpu: 0.05813	lost: 0.25000
total: 0.44362	cap: 0.07487	worker: 0.05306	gpu: 0.05306	cpu: 0.06321	lost: 0.25248
total: 0.44338	cap: 0.07523	worker: 0.05254	gpu: 0.05254	cpu: 0.06136	lost: 0.25425
total: 0.46872	cap: 0.07816	worker: 0.05330	gpu: 0.05330	cpu: 0.06172	lost: 0.27554
total: 0.45397	cap: 0.07776	worker: 0.05527	gpu: 0.05527	cpu: 0.06103	lost: 0.25991
total: 0.44070	cap: 0.07428	worker: 0.05376	gpu: 0.05376	cpu: 0.05658	lost: 0.25608
total: 0.45241	cap: 0.07628	worker: 0.04981	gpu: 0.04981	cpu: 0.05762	lost: 0.26869
total: 0.45581	cap: 0.07713	worker: 0.05325	gpu: 0.05325	cpu: 0.06168	lost: 0.26375
total: 0.46012	cap: 0.07756	worker: 0.05384	gpu: 0.05384	cpu: 0.06561	lost: 0.26312
total: 0.46922	cap: 0.08035	worker: 0.05406	gpu: 0.05406	cpu: 0.06199	lost: 0.27282
total: 0.45355	cap: 0.07557	worker: 0.05396	gpu: 0.05396	cpu: 0.06298	lost: 0.26104
total: 0.44770	cap: 0.07572	worker: 0.05042	gpu: 0.05042	cpu: 0.06098	lost: 0.26059
total: 0.44960	cap: 0.07560	worker: 0.05151	gpu: 0.05151	cpu: 0.05610	lost: 0.26639
total: 0.45817	cap: 0.07646	worker: 0.05186	gpu: 0.05186	cpu: 0.06233	lost: 0.26752
total: 0.44949	cap: 0.07549	worker: 0.05051	gpu: 0.05051	cpu: 0.05906	lost: 0.26443

Figure 21. Execution time for the integrated algorithms.

As the vision-based monitoring methods were not well utilised in actual mining sites, this paper propounded an effective method for detecting mine personnel and mining machinery to HEMM drivers in opencast mines through real-time camera streaming. The model's training accuracy (97%) has been evaluated for performance assessment of the algorithm and implemented with a high-speed GPU for real-time application. The estimated execution time for the whole system is 0.44949 second. In future, the image processing algorithm would be modified for better clarity of the processed image, and an advanced GPU processor would be utilised for faster image processing.

Acknowledgments

The authors are thankful to Dr. P. K. Singh, Director, CSIR-Central Institute of Mining and Fuel Research, Dhanbad, India, for his valuable guidance and for granting permission to publish this paper. The authors are also grateful to the management of National Mineral Development Corporation Limited, Hyderabad, India, for supporting during field studies.

Disclosure statement

No potential conflict of interest was reported by the author(s).

Funding

This research was jointly supported by the Ministry of Electronics and Information Technology, Government of India, and National Mineral Development Corporation Limited, Hyderabad, India, with grant no. 16(1)/2018-ESDA.

References

- [1] A.K. Dash, R.M. Bhattacharjee, P.S. Paula, and M. Tikaderb, *Study and analysis of accidents due to wheel trackless transportation machinery in Indian coal mines – Identification of gap in current investigation system*, Procedia Earth and Planetary Science 11 (2015), pp. 539–547. doi:10.1016/j.proeps.2015.06.056



- [2] A. Nieto, E. Sun, and Z. Li, *Real-time assisted driving in open pit mining operations using Google Earth*, Min. Eng. 62 (2010), pp. 21–26.
- [3] S.N. Lu, H.W. Tseng, Y.H. Lee, Y.G. Jan, and W.C. Lee, *Intelligent safety warning and alert system for car driving*, Tamkang J. Sci. Eng. 13 (2010), pp. 395–404.
- [4] E. Sun and X. Zhang, *3D Assisted driving system for haul trucks in surface mining*, Proceedings of International Conference on Transportation, Mechanical, and Electrical Engineering, Changchun, China, 2011, pp. 363–366. doi:[10.1109/TMEE.2011.6199218](https://doi.org/10.1109/TMEE.2011.6199218)
- [5] T. Ruff, *Evaluation of a radar-based proximity warning system for off-highway dump trucks*, Accid. Anal. Prev. 38, 1 (2006), pp. 92–98. doi:[10.1016/j.aap.2005.07.006](https://doi.org/10.1016/j.aap.2005.07.006)
- [6] R. Spinneker, C. Koch, S.B. Park, and J.J. Yoon, *Fast fog detection for camera-based advanced driver assistance systems*. Proceedings of 17th International IEEE Conference on Intelligent Transportation Systems, Qingdao, China, 2014, pp. 1369–1374. doi:[10.1109/ITSC.2014.6957878](https://doi.org/10.1109/ITSC.2014.6957878)
- [7] N. Hautier, J.P. Tarel, J. Lavenant, and D. Aubert, *Automatic fog detection and estimation of visibility distance through use of an on-board camera*, Machine Vision and Applications. 17, 1 (2006), pp. 8–20. doi:[10.1007/s00138-005-0011-1](https://doi.org/10.1007/s00138-005-0011-1)
- [8] M. Negru and S. Nedevschi, *Image based fog detection and visibility estimation for driving assistance systems*. Proceedings of IEEE 9th International Conference on Intelligent Computer Communication and Processing, Cluj-Napoca, Romania, 2013, pp. 163–168. doi:[10.1109/ICCP.2013.6646102](https://doi.org/10.1109/ICCP.2013.6646102)
- [9] N. Hautiere and D. Aubert, *Contrast restoration of foggy images through Fuse of an on-board camera*, Proceedings of the 8th International IEEE Conference on Intelligent Transportation Systems, Vienna, Austria, 2005, pp. 1090–1095. doi: [10.1109/ITSC.2005.1520203](https://doi.org/10.1109/ITSC.2005.1520203).
- [10] R.T. Tan, *Visibility in bad weather from a single image*, Proceedings of IEEE Conference on Computer Vision and Pattern Recognition, Anchorage, Alaska, USA, 2018, pp. 1–8. doi:[10.1109/CVPR.2008.4587643](https://doi.org/10.1109/CVPR.2008.4587643)
- [11] A. Nieto and K. Dagdelen, *Development of dump edge and vehicle proximity warning system using GPS and wireless network communications to improve safety in open pit mines*, Min. Technol.: Trans. Inst. Min. Metall. 320 (2006), pp. 1–8.
- [12] A. Nieto, *Development of a real-time proximity warning and 3D mapping system based on wireless networks*. Virtual reality graphics, and GPS to improve safety in open-pit mines, Colorado School of Mines. Golden CO, USA, 2001, pp. 176.
- [13] K. Saurabh, S.K. Chaulya, G.M. Prasad, S. Ansari, and D. Kumar, *Assessment of different technologies for improving visibility during foggy weather in mining and transportation sectors*, Int. J. Recent Innov. Trends Comput. Commun. 4, 4 (2016), pp. 31–40. doi:[10.17762/ijritcc.v4i4.1949](https://doi.org/10.17762/ijritcc.v4i4.1949)
- [14] D. Chatterjee and S.K. Chaulya, *Vision improvement system using image processing technique for adverse weather condition of opencast mines*, International Journal of Mining, Reclamation and Environment. 33, 7 (2019), pp. 505–516. doi:[10.1080/17480930.2018.1496886](https://doi.org/10.1080/17480930.2018.1496886)
- [15] J. Ma, X. Fan, S.X. Yang, X. Zhang, and X. Zhu, *Contrast limited adaptive histogram equalization-based fusion in YIQ and HSI color spaces for underwater image enhancement*, Int. J. Pattern Recogn. Artif. Intellig. 32, 7 (2018), pp. 1–27. doi:[10.1142/S0218001418540186](https://doi.org/10.1142/S0218001418540186)
- [16] C. Ramya and S.S. Rani, *A novel method for the contrast enhancement of fog degraded video sequences*, Int. J. Comput. Appl. 54, 13 (2012), pp. 1–5. doi:[10.5120/8623-2489](https://doi.org/10.5120/8623-2489)
- [17] N. Smitha, B.S. Ujwala, P. Manjunatha, and L.S. Chethan, *Contrast limited adaptive histogram equalization and discrete wavelet transform method used for the image*, Int. J. Res. Trends Innov. 2 (2017), pp. 142–146.
- [18] H. Lidong, H. Lidong, H. Lidong, and S. Zebin, *Combination of contrast limited adaptive histogram equalization and discrete wavelet transform for image enhancement*, IET Image Processing. 9, 10 (2015), pp. 908–915. doi:[10.1049/iet-ipr.2015.0150](https://doi.org/10.1049/iet-ipr.2015.0150)
- [19] K. Kim, S. Kim, and K.-S. Kim, *Effective image enhancement techniques for fog-affected indoor and outdoor images*, IET Image Processing. 12, 4 (2018), pp. 465–471. doi:[10.1049/iet-ipr.2016.0819](https://doi.org/10.1049/iet-ipr.2016.0819)
- [20] K. He, J. Sun, and X. Tang, *Single image haze removal using dark channel prior*, IEEE Trans. Pattern Anal. Mach. Intell. 33, 12 (2011), pp. 2341–2353. doi:[10.1109/TPAMI.2010.168](https://doi.org/10.1109/TPAMI.2010.168)
- [21] X. Lv, W. Chen, and I. Shen, *Real-time dehazing for image and video*, Proceedings of 8th Pacific Conference on Computer Graphics & Applications, Hangzhou, 2010, pp. 62–69. doi:[10.1109/PacificGraphics.2010.16](https://doi.org/10.1109/PacificGraphics.2010.16).
- [22] S. Zhang, J. Yao, and W. Ren, *Single image haze removal via joint estimation of detail and transmission*. Proceedings of IEEE International Conference on Multimedia and Expo Workshops, San Diego, USA, 2018, pp. 1–6. doi:[10.1109/ICMEW.2018.8551504](https://doi.org/10.1109/ICMEW.2018.8551504)
- [23] M.Z. Zhu, B.W. He, and L.W. Zhang, *Atmospheric light estimation in hazy images based on color-plane model*, Computer Vision and Image Understanding 165 (2017), pp. 33–42. doi:[10.1016/j.cviu.2017.09.005](https://doi.org/10.1016/j.cviu.2017.09.005)
- [24] H. Tajeen and Z. Zhu, *Image dataset development for measuring construction equipment recognition performance*, Automation in Construction 48 (2014), pp. 1–10. doi:[10.1016/j.autcon.2014.07.006](https://doi.org/10.1016/j.autcon.2014.07.006)
- [25] B. Xiao and S.C. Kang, *Deep learning detection for real-time construction machine checking*. Proceedings of 36th International Symposium on Automation and Robotics in Construction. Banff, Canada, 2019, pp. 1136–1141. doi:[10.22260/ISARC2019/0151](https://doi.org/10.22260/ISARC2019/0151)

- [26] A. Nieto, *The mine of the future: The 5s innovation model for the minerals industry*, Res. Policy 3 (2019), pp. 35–39.
- [27] Glencore, Neil Pollard *Earth Moving Equipment Safety Round Table (EMESRT) PR-5A. Vehicle Interaction Systems Performance Requirements – Revision 2*, Available at <https://emesrt.org/stream/region-4/mature-infra/emesrt-pr-5a-vehicle-interaction-systems-performance-requirements-revision-2/>
- [28] Directorate General of Mines Safety, Ministry of Labour, Government of India, DGMS (Tech) Circular No. 6, 2020, [http://www.dgms.net/DGMS\(Tech\)%20Circular%2006%20of%202020.pdf](http://www.dgms.net/DGMS(Tech)%20Circular%2006%20of%202020.pdf)
- [29] Directorate General of Mines Safety, Ministry of Labour, Government of India, DGMS (Tech) Circular (MAMID) No. 8, 2020, <https://indsteel.org/pdf/raw-materials/DGMS%20Circular%20on%20Recommendations%20of%2012th%20National%20Conference%20on%20Safety%20in%20Mines.pdf>
- [30] E. Reinhard, M. Adhikhmin, B. Gooch, and P. Shirley, *Color transfer between images*, IEEE Computer Graphics and Applications. 21, 4 (2001), pp. 34–41. doi:[10.1109/38.946629](https://doi.org/10.1109/38.946629)
- [31] H. Anton, *Elementary Linear Algebra*, 7th, New York, John Wiley & Sons, 1994, pp. 170–171.
- [32] H. Zhu, X. Wen, F. Zhang, X. Wang, and G. Wang, *Homography estimation based on order-preserving constraint and similarity measurement*, IEEE Access 6 (2018), pp. 28680–28690. doi:[10.1109/ACCESS.2018.2837639](https://doi.org/10.1109/ACCESS.2018.2837639)
- [33] T. Xiang, G.S. Xia, and L. Zhang, *Image stitching with perspective-preserving warping*, Proceedings of ISPRS Annals of Photogrammetry, Remote Sensing and Spatial Information Sciences, Prague, Czech Republic. 3 (2016), pp. 287–294. doi:[10.5194/isprs-annals-III-3-287-2016](https://doi.org/10.5194/isprs-annals-III-3-287-2016)
- [34] O. Russakovsky, J. Deng, H. Su, J. Krause, S. Satheesh, S. Ma, Z. Huang, A. Karpathy, A. Khosla, M. Bernstein, A.C. Berg, and L. Fei-Fei, *ImageNet large scale visual recognition challenge*, Int. J. Comput. Vis. 115, 3 (2015), pp. 211–252. doi:[10.1007/s11263-015-0816-y](https://doi.org/10.1007/s11263-015-0816-y)
- [35] A.G. Howard, M. Zhu, B. Chen, D. Kalenichenko, W. Wang, T. Weyand, M. Andreetto, and H. Adam, *Mobilenets: Efficient convolutional neural networks for mobile vision applications*, ArXiv. abs/1704.04861, 2017. <https://arxiv.org/abs/1704.04861v1>
- [36] W. Liu, D. Anguelov, D. Erhan, C. Szegedy, S. Reed, C.Y. Fu, and A.C. Berg, *SSD: Single Shot Multibox Detector*, Springer, Cham-Lecture Notes in Computer Sci, 21–37, 2016. doi:[10.1007/978-3-319-46448-0_2](https://doi.org/10.1007/978-3-319-46448-0_2).
- [37] M. Yang, K. Hu, Y. Du, Z. Wei, Z. Sheng, and J. Hu, *Underwater image enhancement based on conditional generative adversarial network*, Signal Processing: Image Communication 81 (2020), pp. 115723. doi:[10.1049/iet-ipr.2015.0150](https://doi.org/10.1049/iet-ipr.2015.0150)
- [38] A. Younis, L. Shixin, S. Jn, and Z. Hai, *Real-time object detection using pre-trained deep learning models MobileNet-SSD*. Proceedings of 6th International Conference on Computing and Data Engineering, Sanya, China, 2020, pp. 44–48. doi:[10.1145/3379247.3379264](https://doi.org/10.1145/3379247.3379264)
- [39] M.H. Niloy, *Detect Excavators using Computer Vision. Excavator Dataset*, 2019; dataset available at <https://www.kaggle.com/ashrafminhaj/excavator>
- [40] J. Huang, V. Rathod, C. Sun, M. Zhu, A. Korattikara, A. Fathi, I. Fischer, Z. Wojna, Y. Song, S. Guadarrama, and K. Murphy, *Speed/accuracy trade-offs for modern convolutional object detectors*. Proceedings of Computer Vision and Pattern Recognition, Honolulu, HI, US, 2017, pp. 1137–1143. doi:[10.1109/CVPR.2017.351](https://doi.org/10.1109/CVPR.2017.351)
- [41] R. Kohavi, *A study of cross-validation and bootstrap for accuracy estimation and model selection*, Proceedings of the 14th International Joint Conference on Artificial Intelligence, Montreal, Quebec, Canada, 1995, pp. 1137–1143. doi:[10.5555/1643031.1643047](https://doi.org/10.5555/1643031.1643047)